ChemElectroChem

Research Article
doi.org/10.1002/celc.202201002

Chemistry Europe
European Chemical Societies Publishing

www.chemelectrochem.org

Special Collection

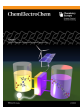

A Neutral-pH Aqueous Redox Flow Battery Based on Sustainable Organic Electrolytes

Jorge Montero, Williane da Silva Freitas, Barbara Mecheri, Mattia Forchetta, Pierluca Galloni, Silvia Licoccia, and Alessandra D'Epifanio*[a]

Aqueous organic redox flow batteries (AORFBs) have gained increasing attention for large-scale storage due to the advantages of decoupled energy and power, safe and sustainable chemistry, and tunability of the redox-active species. Here, we report the development of a neutral-pH AORFB assembled with a highly water-soluble ferrocene 1,1-disulfonic disodium salt (DS–Fc) and two viologen derivatives, 1,1′-bis(3-sulfonatopropyl)-viologen (BSP–Vi) and Bis(3-trimethylammonium)propyl viologen tetrachloride (BTMAP–Vi). Synthesized electrolytes showed excellent redox potential, good diffusion coefficient, and a good transfer rate constant. In particular, BSP–Vi has a more negative redox potential (-0.4 V) than BTMAP–Vi (−0.3 V) and faster kinetics; therefore, it was selected to be assembled in an AORFB as anolyte, coupled with DS–Fc as catholyte.The resulting AORFB based on BTMAP–Vi/DS–Fc and BSP–Vi/DS–Fc redox couple had a high cell voltage (1.2 V and 1.3 V, respectively) and theoretical energy density (13 WhL^{-1} and 14 WhL^{-1} respectively) and was able to sustain 70 charge-discharge cycles with energy efficiency as high as 97%.

Introduction

Developing low-cost and safe large-scale energy storage systems is an urgent challenge to meet the demand for the efficient use of renewable energy.[1] Redox flow batteries (RFBs) represent a promising technology to address this challenge, thanks to their intrinsic safety, low cost, long-term durability, and independent energy/power sizing.[2] An RFB uses aqueous or non-aqueous solutions of redox-active couples pumped to the cell stack from external tanks.[3,4] Compared to non-aqueous RFBs, aqueous RFBs have already demonstrated successful scale-up, for they do not require a stringent system design for safety considerations.[5] First-generation aqueous RFBs rely on transition metal-based electrolytes. Among them, vanadium redox flow batteries (VRFBs) are already commercially available, accounting for several large-sized systems (commercial and demonstration projects) installed across the globe.[6–8] However, the high cost of vanadium hinders the widespread deployment of VRFBs.

As an emerging technology, aqueous organic redox flow batteries (AORFBs) exploit the reversible redox reaction of organic and organometallic compounds. Being made of earth-abundant elements such as C, H, N, O, P and S, such compounds potentially have lower and more stable costs than vanadium.[9,10] Furthermore, molecular engineering strategies enable the structural tailoring of organic electrolytes to modulate the redox potential and solubility and enhance kinetics and stability under operating conditions.[11–15] Ferrocene, quinone, viologen, phenazine, phenothiazine, 2,2,6,6-tetramethyl-1-piperidinyloxy (TEMPO), azobenzene, alloxazines, and redox-active coordination polymers[16] are possible candidates as electrolytes for AORFBs.[17,18]

In addition to vanadium cost, the use of highly concentrated sulfuric acid as a supporting electrolyte on VRFBs can cause problems due to its corrosive nature, leading to the degradation of the battery components.[19] Some AORFBs also use corrosive alkaline and acidic solutions that, besides deterioration of the system, jeopardize the stability of the redox-active materials giving rise to irreversible capacity loss.[20]

For this reason, the investigation of neutral pH electrolytes that can avoid RFB components' degradation and increase their active materials' stability is crucial to achieving long-term cycling stability. Generally, a highly oxidative and corrosive environment is highly demanding and requires robust and withstand materials. On the other hand, a neutral environment allows inexpensive and easy-to-manufacture materials that significantly reduce costs by favoring the large-scale commercialization of AORFBs.

Viologen's solubility and stability at neutral pH open the possibility of operation without the involvement of highly alkaline or acidic solutions, leading to higher safety in handling and fewer requirements on battery components.[18,21,22] In addition, viologen offers the advantages of fast redox kinetics, decent redox potential (< -0.3 V *vs.* SHE), and facile synthesis.[23–25] First-generation viologen-based RFBs utilized methyl viologen (MV), but the dimerization of an intermediate

[a] *Dr. J. Montero, Dr. W. da Silva Freitas0000-0001-9041-8168, Prof. B. Mecheri, Dr. M. Forchetta, Prof. P. Galloni, Prof. S. Licoccia, Prof. A. D'Epifanio*
Department of Chemical Science and Technologies
University of Rome Tor Vergata
Via della Ricerca Scientifica, 00133 Rome, Italy
E-mail: alessandra.d.epifanio@uniroma2.it
Homepage: 0000-0001-9041-8168

Supporting information for this article is available on the WWW under https://doi.org/10.1002/celc.202201002

Special Collection *An invited contribution to a Special Collection dedicated to Giornate dell'Elettrochimica Italiana 2022 (GEI2022)*

MV radical cation jeopardized the performance of MV-based RFBs, leading to a high-capacity loss over cycling. Aziz and co-workers[26] adopted a molecular engineering approach to prevent dimerization, exploiting the establishment of coulombic repulsion due to adding quaternary ammonium groups to the viologen core. Other authors adopted a similar approach, obtaining modified MV-based RFBs with a much lower capacity loss than the first-generation MV-RFBs.[27] Although the recent progress in developing viologen-based neutral AORFBs[28–36] the influence of the viologen's substituents on their redox behavior and electrochemical stability once coupled with a positive electrolyte in neutral AORFBs needs to be further explored.

As far as the positive electrolyte (catholyte) is concerned, ferrocyanide is the most promising catholyte in terms of stability and redox potential for near-neutral AORFBs.[11,37,38] However, to move towards fully organic or organic/organometallic AORFBs, ferrocene (Fc) can be considered a promising redox-active organometallic compound used as a catholyte. Fc exhibits very reversible oxidation and reduction, and its chemistry is well understood, but it has limited water solubility, affecting its application in aqueous systems. For this reason, the ferrocene/ferrocenium ion redox couple has found application as model chemistry for non-aqueous redox flow battery research.[39–42] Previous reports dealt with modifying hydrophobic Fc with hydrophilic moieties, resulting in an increased solubility in an aqueous solution.[43–49] Z. Zhao et al.[50] used 1,1′-bis(sulfonate)-ferrocene dianion disodium salt pared with the anthraquinone-2,7-disulfonic acid disodium salt; on the other hand, ferrocene decomposed under the acidic conditions used to stabilize the anthraquinone.[42] Considering our expertise in synthesis and applications of electro-active molecules, in particular metallocenes,[51–54] we synthesized in this work the 1,1′-bis(sulfonate)-ferrocene dianion disodium salt (DS–Fc) and two viologen-derivatives, as catholyte and anolyte, respectively, to produce a sustainable neutral-pH AORFB. The performances of the synthesized electrolytes were evaluated in terms of solubility, degradation capacity, retention, and electrical power generation. The results indicated a high cell voltage and theoretical energy density.

Results and Discussion

Ferrocenes solubility can be tuned by functionalizing one or both cyclopentadienyl rings with polar groups, enhancing their water solubility up to 0.5 M.[55] The addition of electron-withdrawing groups, such as sulphonic or carboxylic groups, also makes the ferrocene oxidation more difficult and leads to the increase of the redox potential of the ferrocene/ferrocenium couple, opening the possibility of increasing the battery's overall potential.[56] In this work, the ferrocene has been functionalized with SO_3^- group to obtain the 1,1-disulfonic disodium salt (DS–Fc) (Figure 1a).

Viologens exist in three oxidation states, $Vi^{2+} \rightleftharpoons Vi^{+\bullet} \rightarrow Vi^0$, where the first reduction step is highly reversible and the second one is irreversible. The potential difference between the first and second reduction is very low, making it impossible to avoid the second reduction process.[57] The alkylation of the viologen can increase this gap between the reductions. $Vi^{+\bullet}$ species can also suffer from reoxidation by collision with other viologen molecules. This collision can be avoided by adding charged groups to the alkyl chain, increasing the electrostatic repulsion.

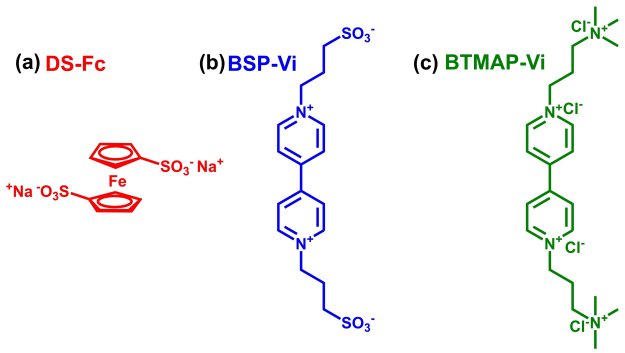

Figure 1. Chemical structure of (a) ferrocene 1,1-disulfonic disodium salt (DS–Fc), (b) 1,1′-bis(3-sulfonatopropyl)-viologen (BSP–Vi) and (c) Bis(3-trimethylammonium)propyl viologen tetrachloride (BTMAP–Vi).

We prepared and investigated two different viologen derivatives: 1,1′-bis(3-sulfonatopropyl) viologen (BSP–Vi) (Figure 1b) and (3-trimethylammonium)propyl viologen tetrachloride (BTMAP–Vi) (Figure 1c).

The solubility of BTMAP–Vi and BSP–Vi is expected to be similar, reaching 2 M concentration.[58] The molecular structures of the synthesized DS–Fc, BTMAP–Vi and BSP–Vi were confirmed by ^{1}H NMR (Figure S1).

The electrochemical properties of the active materials were investigated by cyclic voltammetry (CV) analysis in 0.5 M $NaNO_3$ aqueous solution (Figure 2). $NaNO_3$ as a supporting electrolyte aimed to alleviate undesired nucleophilic attacks to the DS–Fc which anions, such as chloride, can promote via the nucleophilic conversion of Fc^+ into $FeCl_4^-$.[59] Nevertheless, either KCl or NaCl has been widely used as supporting salts in previous reports.[54,56,60,61] We prepared DS–Fc aqueous solutions containing either KCl or $NaNO_3$ as supporting electrolytes. As expected, we found improved stability of the DS–Fc solution with $NaNO_3$

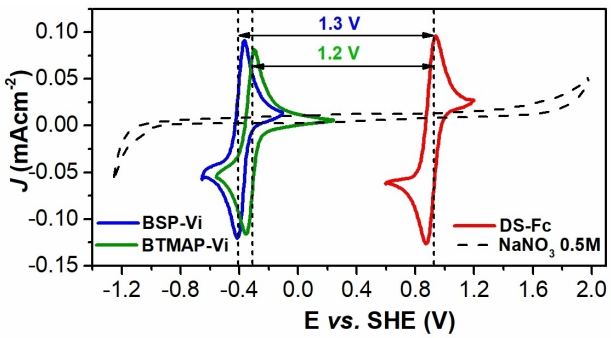

Figure 2. CVs at a 10 mVs^{-1} scan rate for BSP–Vi ($E_{1/2} = -0.40$ V), BTMAP–Vi ($E_{1/2} = -0.30$ V), DS–Fc ($E_{1/2} = 0.90$ V) in 0.5 M $NaNO_3$ aqueous electrolyte, and 0.5 M $NaNO_3$, hydrogen evolution reaction (HER, −1.00 V) and oxygen evolution reaction (OER, 1.50 V).

as compared to NaCl (Figure S2). Moreover, previous reports indicated that some ferrocene derivatives, when exposed to light, might lead to photodecomposition;[62] for this reason, we studied our sample's stability by preparing two DS–Fc solutions in $NaNO_3$; one of them was left in contact with ambient light and the other one was kept in the dark (Figure S3).

After one week, the solution in contact with light showed a precipitate resulting from the degradation of DS–Fc. This phenomenon of photodecomposition has not been discussed in previous works using ferrocene derivatives as electrolytes for RFBs. As a result, all the following electrochemical tests were carried out by avoiding contact with light.

CV of DS–Fc revealed a reversible $Fe^{2+} \rightleftharpoons Fe^{3+}$ redox couple reaction with half-wave potential ($E_{1/2}$) 0.90 V *vs.* SHE. CV of the two viologen-derivatives indicated a reversible $Vi^{2+} \rightleftharpoons Vi^{+\bullet}$ redox couple reaction with $E_{1/2}$ of −0.40 V *vs.* SHE for the BSP–Vi and −0.30 V *vs.* SHE for BTMAP–Vi (Figure 2). The substitution of the quaternary ammonium groups with sulphonic groups negatively shifted the $Vi^{2+}/Vi^{+\bullet}$ redox potential by 100 mV.

Based on these results, the AORFB based on BTMAP–Vi/DS–Fc couple has an expected open-circuit voltage (OCV) value of 1.2 V, while the AORFB based on BSP–Vi/DS–Fc has a 1.3 V OCV. The latter represents one of the highest cell voltages reported in the literature for similar AORFBs (Table 1).

Moreover, based on solubility and cell voltage, the AORFBs based on BTMAP–Vi/DS–Fc and BSP–Vi/DS–Fc have energy densities of 13.0 and 14.0 WhL^{-1}, respectively, and a theoretical capacity of 13.4 AhL^{-1}.

We further analyzed the electrochemistry of BSP–Vi, DS–Fc, and BTMAP–Vi by performing Linear Sweep Voltammetry (LSV) analysis using a rotating disk electrode (RDE) setup. Figure 3(a), 3(b), and S4(a) show LSVs recorded at different electron rotation speeds for BSP–Vi, DS–Fc, and BTMAP–Vi, respectively. The polarization curves of all samples showed a well-defined diffusion-limited current plateau at all rotation speeds. They were analyzed through the Koutecký-Levich (K–L) theory[65] to evaluate the diffusion coefficient (D) of the redox-active species., as described in the supporting information (Equation S1). Figure 3(c), 3(d) and S4(b) show the corresponding K–L

Table 1. Performance comparison of active redox couples operating in neutral-pH AORFBs.

Anolyte	Catholyte	Electrolyte	Cell voltage [V]	Capacity [AhL^{-1}]	Energy density [WhL^{-1}]	Capacity fade	Capacity retention	Ref.
2,7-AQDS	DS-Fc	$NaNO_3$ 1 M	1.1	8	4.42	–	25%/total	[50]
BTMAP-Vi	TPABPy	none	1,29	37.6	19	–	99.98%/cycle	[63]
M–Vi	4HO-TEMPO	NaCl 1 M	1.25	2.68	3.35	–	89%/total	[60]
M–Vi	NCl-Fc	NaCl 2 M	1.05	53.5	35.8	–	99.99%/cycle	[64]
BTMAP-Vi	BTMAP-Fc	NaCl 0.5 M	0.75	26	20	0.0057%/cycle	99.99%/cycle	[61]
BSP-Vi	DS-Fc	$NaNO_3$ 0.5 M	1.3	13.4	14	0.24%/cycle	90%/total; 98.35%/cyle	This work

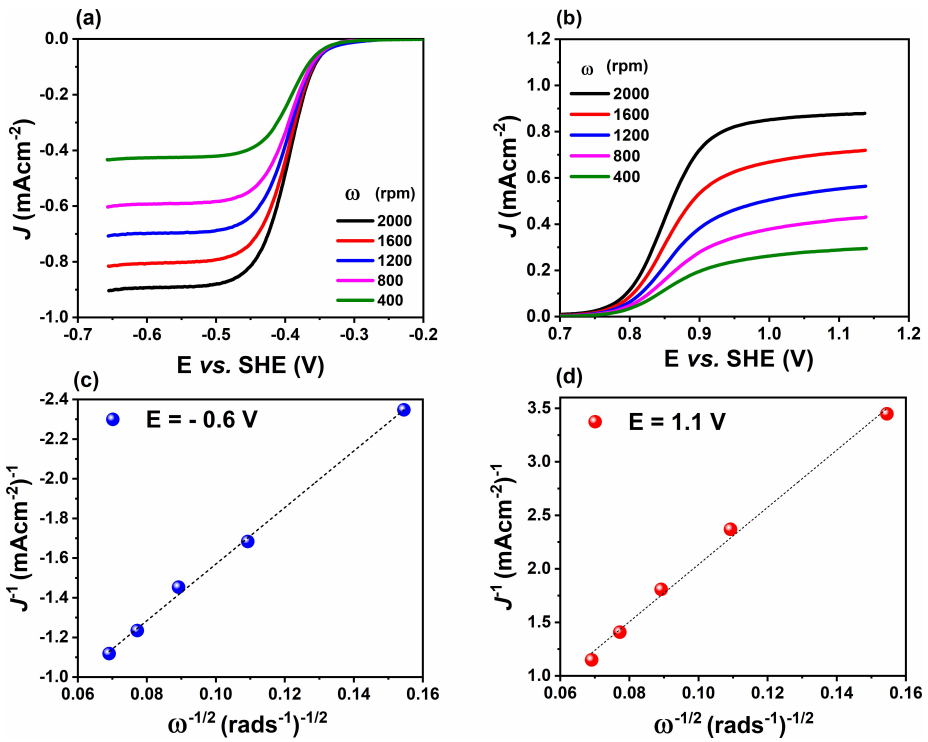

Figure 3. LSV curves at different rotation speeds and a 10 mVs^{-1} potential scan rate acquired in 0.5 M $NaNO_3$ aqueous electrolyte and Koutecký-Levich (J^{-1} *vs.* $\omega^{-1/2}$) plot, respectively, for (a, c) BSP–Vi and (b, d) DS–Fc at a 2 mM concentration.

plots of BSP–Vi, DS–Fc, and BTMAP–Vi, respectively, that yielded diffusion coefficients of 4.4×10^{-6} cm^2s^{-1} (BSP–Vi), 1.7×10^{-6} cm^2s^{-1} (DS–Fc), 3.5×10^{-6} cm^2s^{-1}.

These values are aligned or even higher than those reported in the literature (Table S1), indicating that molecular diffusion of the BSP–Vi and DS–Fc species towards the electrode surface is favored in the operating conditions (0.5 M $NaNO_3$), contributing to the redox reactions kinetic.

Nicholson's method was also adopted to estimate BTMAP–Vi, BSP–Vi, and DS–Fc redox electron transfer rate constant (k^0), by extrapolating the peak(E_{pc})-peak(E_{pa}) separation (ΔE_p) from CV analysis. This method introduces a dimensionless parameter, Ψ, that indicates electrochemical reversibility. When Ψ is equal to 20 the redox process is considered reversible, and this value can be assumed when $\Delta E_p \leq 61$ mV. The relation between Ψ and k^0 is given by Equation S2.[66,67]

The redox reactions for both BTMAP–Vi and BSP–Vi displayed a constant ΔE_p of 45 and 47 mV, respectively, over the different scan rates investigated (10 to 350 mV). DS–Fc had a ΔE_p of 57 mV, corroborating a fast and reversible redox process. The k^0 values for BTMAP–Vi, BSP–Vi, and DS–Fc were 4.1×10^{-2} cms^{-1} 4.6×10^{-2} cms^{-1}, and 2.9×10^{-2} cms^{-1} respectively, which are in the range found in the literature for others high-active viologen- and ferrocene-derivatives (Table S1). The good solubility in the aqueous electrolyte, high diffusion coefficient, and k^0 values, indicate that the synthesized materials can be good anolyte and catholyte candidates in neutral-pH RFBs.

Based on superior $E_{1/2}$, D, and k^0 values, BSP–Vi has a higher electrochemical performance than BTMAP–Vi. Moreover, BSP–Vi presents further advantages compared to the BTMAP–Vi, starting from the more straightforward synthesis procedure, which requires fewer synthetic steps than BTMAP–Vi. The presence of sulfonic groups in BSP–Vi is also expected to promote an enhanced affinity with the cationic membrane used in the AORFB as a separator. By contrast, the cationic nature of BTMAP–Vi could cause an unequal distribution of charged ions on either side of the membrane due to the Gibbs-Donnan effect.[68]

For those reasons, an AORFB based on BSP–Vi/DS–Fc as redox couples was assembled, and its electrochemical performance was evaluated. Permeability tests were carried out using the H-cell set-up (Figure S5), equipped with a Nafion 212 membrane. According to the tests (Figure S6 and Figure S7), permeability phenomena were not observed in the case of DS–Fc, and only a slight crossover rate was observed for BSP–Vi, with a permeability coefficient of 1.03×10^{-8} cm^2min^{-1} calculated according to the Equation S3. AORFB's electrochemical tests were performed with a 30 mL solution of 10 mM DS–Fc as catholyte and 10 mM BSP-Vi as anolyte in 0.5 M $NaNO_3$ as supporting electrolyte and a Nafion 212 as membrane: resulting in a theoretical capacity of 268 $mAhL^{-1}$. The battery was cycled at the C-rates of 1.33, 2.67, and 5.33 $mAcm^{-2}$ as similar C-rates can be found in the literature.[50] Figure 4(a) shows typical voltage charge and discharge profiles as a function of capacity: the DS–Fc/BSP–Vi AORFB displayed a high working voltage (> 1.0 V) and a capacity of 150 $mAhL^{-1}$, which represents 60% of the theoretical capacity at 1.33 $mAcm^{-2}$ (C/1.5), that decrease at 45% and 35% with current increases at 2.67 (C/1.33) and 5.33 $mAcm^{-2}$ (1.5 C), respectively.

The current rate performance was investigated under different C/rate and plotted in Figure 4(b). Five charge and discharge

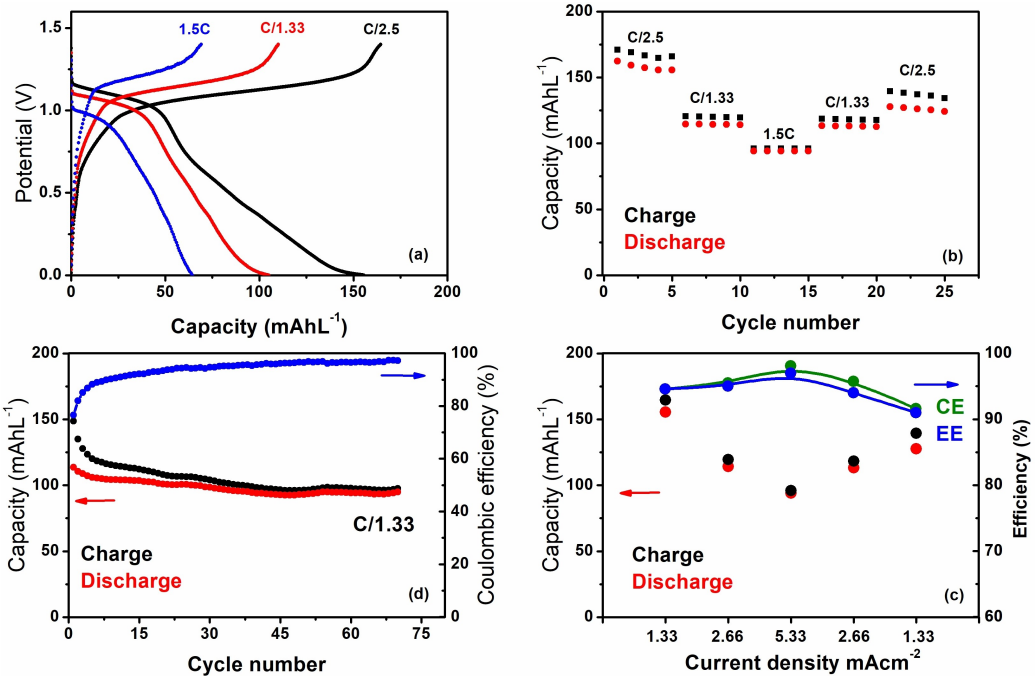

Figure 4. Battery studies of 10 mM DSFc/BSPVi AORFB. (a) Voltage profiles at different current densities 1.33 $mAcm^{-2}$ (C/1.5), 2.67 $mAcm^{-2}$ (C/1.33) and 5.33 $mAcm^{-2}$ (1.5 C). (b) Battery charge-discharge capacity at different current densities. (c) Coulombic Efficiency (CE) and Energy Efficiency (EE) at different current densities. (d) charge-discharge capacity, and Coulombic efficiency versus cycle number at C/1.33.

cycles were acquired for each current density with cut-off voltages of 1.5 V for the charging process and 0.01 V for the discharging process. At all current densities, the capacity is stable, while the coulombic efficiency (CE) increases from 94.6% to 98% when the current increases (Figure 4c). This trend is confirmed when the current is decreased to the initial values, CE decreasing as current density decreases. At a lower current density (C/2.5), the electrolyte is exposed to a high voltage for more time, which could favor redox couples' electrochemical degradation during the tests.

This partial degradation of DS–Fc can be due to sulphonic groups directly connected to the cyclopentadienyl rings, which facilitate a nucleophilic attack on the Fc molecule, as previously observed.[69] The Energy efficiency (EE) data confirm the CE trend; EE increases with the current density increase reaching 97% at 1.5 C. This is consistent with a high D and k^0 of both BSP–Vi and DS–Fc and a low area-specific resistance (1.01 Ωcm^2), calculated by high-frequency electrochemical impedance spectroscopy at an open-circuit voltage (Figure S11).

The cell stability was evaluated by galvanostatic cycling at C/1.33 between 1.5-0.01 V for 70 cycles (Figure 4d). A capacity loss during the first cycles was observed, which could be ascribed to the photodecomposition of DS–Fc during the assembly of the battery, which occurred in the presence of air and light.

It is reasonable to ascribe to decomposition phenomenon to the formation of cyclopentadienyl-based radicals that can react with the ferrocenium cation during cycling, in good agreement with previous reports.[69] After this, the discharge capacity remained constant throughout the test at around 100 mAh; moreover, the average CE after the first cycles were ~96%.

Capacity retention was calculated as the ratio between discharge capacity at the 70th cycle and discharge capacity at the 1st cycle. A 90% capacity retention was obtained, corresponding to a capacity fade of 0.24% per cycle and 0.23% per hour, confirming the good electrochemical performance of both electrolytes under AORFB operating conditions.

Conclusion

Sustainable and tuneable active organometallic and organic compounds electrolytes based on ferrocene (DS–Fc) and viologen (BSP–Vi, and BTMAP–Vi) have been synthesized and studied for applications in a neutral-pH aqueous organic redox flow battery. The stability of the redox active molecules was investigated and optimized in terms of supporting electrolyte and operating conditions of the AORFB. Among the two Vi derivatives, BSP–Vi performs better than BTMAP–Vi, due to more negative redox potential, and enhanced kinetics, as demonstrated by the electrochemical characterization in a half-cell. Considering also that the BSP–Vi can be prepared with a more straightforward synthesis procedure, an AORFB battery based on BSP–Vi/DS–Fc was assembled and characterized.

Permeability tests revealed that DS–Fc has no crossover through the Nafion 212 membrane, and the permeability coefficient of BSP–Vi is as low as 1.03×10^{-8} $cm^2 min^{-1}$.

The BSP–Vi/DS–Fc AORFB resulted in a high cell voltage of 1.30 V, one of the highest obtained for AORFB, and a good theoretical energy density (14 WhL^{-1}). Finally, the cycling behavior of BSP–Vi/DS–Fc AORFB was investigated, leading to high coulombic efficiency (up to 98% at 1.5 C) and capacity retention of 90% after 70th.

Experimental Section

All reagents were purchased from Sigma-Aldrich. Ferrocene had a reagent grade and a purity of 98%. Acetic anhydride had a purity of >99%. Sodium hydroxide pellets (anhydrous) had a reagent grade of >98%. Sulfuric acid ACS reagent with a 95–98% purity. Toluene was ACS purity, 99.5%. 1,3-propane sultone has a reagent grade of 98%.

Preparation of ferrocene 1,1-disulfonic disodium salt (DS-Fc): 9.5 g of ferrocene (51 mmol) were dissolved in acetic anhydride under magnetic stirring at room temperature, yielding an orange solution. Sulfuric acid (5 mL) was added dropwise, keeping the temperature below 45 °C. The mixture was stirred for 2 hours at room temperature and set aside to allow the product's precipitation, which was collected by filtration. The product was washed first with acetic anhydride, then pentane, and filtered under vacuum. The yellow solid, which turned dark yellow with drying, was dissolved in distilled water (DW) and neutralized with sodium hydroxide until neutral pH. The solution was then freeze-dried, giving 16.85 g (43 mmol, 85% yield) of a free-flowing yellow powder (DS–Fc).[56] Figure S8 shows the synthesis route of DS–Fc.

Preparation of 1,1′-bis(3-sulfonatopropyl)-viologen (BSP-Vi): 726 mg of 4,4′-bipyridine (4.61 mmol) and 1.12 g of propanesultone (9.22 mmol – 2 equivalents) were refluxed in toluene, for 3 hours, in an inert atmosphere. Afterward, the white precipitate obtained was collected by vacuum filtration, rinsed with acetonitrile, and dried under vacuum, giving 1.63 g (41 mmol, 88% yield) of a white powder (BSP–Vi).[58] Figure S9 shows the synthesis route of BSP–Vi.

Preparation of Bis(3-trimethylammonium)propyl viologen tetrachloride (BTMAP-Vi): 99.2 g of 1-bromo-3-chloropropane (630 mmol) was dissolved in 50 mL of a 4.2 M trimethylamine solution in ethanol. After stirring at room temperature for 15 hours, the reaction mixture was diluted with diethyl ether, and the suspended solid was collected by vacuum filtration. The resulting white powder and 15.62 g of 4,4′-bipyridine (100 mmol) were suspended in anhydrous DMF and heated to reflux under argon. Upon heating, all solids dissolved, followed by the rapid formation of a pale-yellow precipitate, which turned greenish after 1 hour. The reaction was cooled to room temperature, followed by the addition of isopropanol; the solid was then collected by vacuum filtration, rinsed first with isopropanol, then acetone, and finally dried under vacuum, obtaining (3-trimethylammonium)propyl viologen dibromide dichloride. An aqueous solution of (3-trimethylammonium)propyl viologen dibromide dichloride was passed through an Amberlite IRA-900 resin (chloride form). The resin was washed with distilled water until the eluted solution produced no precipitate upon testing with an aqueous $AgNO_3$ solution. The eluted solution was evaporated under vacuum, giving 290 g (580 mmol, 92% yield) of (3-trimethylammonium)propyl viologen tetrachloride (BTMAP–Vi) as a brownish solid.[61] Figure S10 shows the synthesis route of BTMAP–Vi.

Physicochemical and electrochemical characterization of Ferrocene- and Viologen-derivatives: ^{1}H-NMR spectra have been recorded with Bruker Avance 700 MHz in D_2O and DMSO-d_6, at a sample concentration of 1.0 mgmL^{-1}. The electrochemical characterization of the prepared materials was carried out by using a three-electrode electrochemical cell equipped with a rotating disk glassy carbon electrode (AFE6R2GCPT, Pine Research Instrumentation, area = 0.196 cm^2) as a working electrode (WE), a platinum wire (Amel 805/SPG/12), and a saturated calomel electrode (SCE, Amel 303/SCG/12) as a counter electrode, and reference electrodes, respectively. The measurements were acquired with a VMP3 Potentiostat (BioLogic Science Instruments) controlled by a computer through EC-Lab V10.18 software. Potential values for all electrochemical tests were measured vs. SCE and converted to the standard hydrogen electrode (SHE) scale. Electrochemical measurements were performed in an 0.5 M $NaNO_3$ aqueous solution after purging N_2 gas for 20 min. CV was carried out at 10 mVs^{-1} potential scan rate in a 2 mM solution of Ferrocene- and Viologen-derivatives in 0.5 M $NaNO_3$. Linear sweep voltammetry (LSV) curves were also recorded at a scan rate of 10 mVs^{-1} and different electrode rotation speed (400, 800, 1200, 1600, and 2000 rpm), from 0.3 to 0.9 V vs. SHE. CV and LSV curves were recorded over three runs to ensure repeatability.

Permeability tests. The permeability test was carried out in a H-cell (Figure S5). Compartment A contained a solution of the active material (10 mM) in 0.5 M $NaNO_3$ and compartment B had a 0.5 M $NaNO_3$ solution. The active material concentration variation in compartment B was measured by UV-Vis (Cary 50 Scan, Varian, Palo Alto, California, USA), as shown in Figures S6 and S7. The permeability coefficient was calculated according to Equation S3.

Redox Flow battery tests. AORFB tests were carried out at room temperature and argon atmosphere employing 30 mL of a 10 mM solution of DS–Fc and BSP–Vi, with 0.5 M $NaNO_3$ as supporting electrolyte in water solution. The cell was assembled by sandwiching Nafion N212 between two electrodes composed of three stacked carbon felts (Sigracet SGL 39AA), placed between two graphite plates with serpentine flow fields (Poco Graphite, Fuel Cell Technologies, Albuquerque, New Mexico, USA). The active area was 2.25 cm^{2,} and two gaskets in Viton rubber of appropriate thickness were used to seal the cell. Each electrode was pre-treated at 400 °C for 24 hours. The N212 membrane was also pre-activated by immersion at 60 °C in the following solutions: first an aqueous H_2O_2 (3.0 vol.%) and then an aqueous solution 0.5 M H_2SO_4, for 1 h each. Lastly, the membranes were stored immersed in the electrolyte solution for 24 hours. A flux rate of 100 mLmin^{-1} was set on both sides using KNF diaphragm pumps (KNF, Trenton, NJ, USA). The AORFB was assembled by introducing all materials and components inside a glove box with an argon atmosphere. Before cycling, argon was fluxed into the tanks for 1 hour to avoid residual oxygen inside the solutions. The electrochemical studies of the battery were accomplished by galvanostatic charge-discharge cycling employing a multi-channel potentiostat VMP3 (Bio-Logic Science Instruments, Seyssinet-Pariset, France) controlled by a computer through EC-Lab V10.18 software. The ASR (Area-specific resistance) was measured by electrochemical impedance spectra EIS, shown in Figure S11. The battery was cycled with the current densities of 1.33 mAcm^{-2} that correspond at C/rate C/2.5, 2.68 mAcm^{-2} (C/1.33) and 5.33 mAcm^{-2} (1.5 C) with cut off voltages of 1.4 V and 0.01 V. Electrochemical parameters, such as theoretical capacity, theoretical energy density, C rates, coulombic efficiency, and energy efficiency were calculated according to Equations S4 to S9.

Acknowledgements

This work has received funding from Regione Lazio (Italy) through the project POR FESR LAZIO 2014–2020, N° A0375-2020-36492.

Conflict of Interest

The authors declare no conflict of interest.

Data Availability Statement

The data that support the findings of this study are available from the corresponding author upon reasonable request.

Keywords: Aqueous Redox Flow Battery · Organo-metallic Electrolyte · Neutral-pH environment · Viologen- and Ferrocene-derivatives · Electrochemical energy storage

[1] Z. Zhang, X. Xiao, W. Yu, Z. Zhao, P. Tan, *Nano Lett.* **2022**, *22*, 7527–7534.
[2] P. Arévalo-Cid, P. Dias, P. Mendes, P. Azevedo, *Sustain. Energy Fuels* **2021**, *5*, 5366–5419.
[3] F. Chu, M. Su, G. Xiao, Z. Tan, G. Yang, *Ind. Eng. Chem. Res.* **2022**, *61*, 2915–2925.
[4] F. Wang, G. Xiao, F. Chu, *Chem. Eng. J.* **2023**, *451*, DOI 10.1016/j.cej.2022.138619.
[5] M. L. Perry, K. E. Rodby, F. R. Brushett, *ACS Energy Lett.* **2022**, *7*, 659–667.
[6] C. Minke, T. Turek, *J. Power Sources* **2018**, *376*, 66–81.
[7] J. H. Vinco, A. E. E. da C. Domingos, D. C. R. Espinosa, J. A. S. Tenório, M. Dos P. G. Baltazar, *J. Energy Storage* **2021**, *43*, 103180.
[8] Z. Liu, R. Li, J. Chen, X. Wu, K. Zhang, J. Mo, X. Yuan, H. Jiang, R. Holze, Y. Wu, *ChemElectroChem* **2017**, *4*, 2184–2189.
[9] X. Li, Y. Wang, L. Lv, G. Zhu, Q. Qu, H. Zheng, *Energy Materials* **2022**, *2*, 200014.
[10] T. Huang, M. Long, J. Xiao, H. Liu, G. Wang, *Energy Materials* **2022**, *1*, 100009.
[11] D. G. Kwabi, Y. Ji, M. J. Aziz, *Chem. Rev.* **2020**, *120*, 6467–6489.
[12] Y. Liu, Q. Chen, X. Zhang, J. Ran, X. Han, Z. Yang, T. Xu, *Curr. Opin. Electrochem.* **2022**, *32*, 100895.
[13] X. Zu, L. Zhang, Y. Qian, C. Zhang, G. Yu, *Angew. Chem. Int. Ed.* **2020**, *59*, 22163–22170; *Angew. Chem.* **2020**, *132*, 22347–22354.
[14] R. P. Fornari, M. Mesta, J. Hjelm, T. Vegge, P. De Silva, *ACS Materials Lett.* **2020**, *2*, 239–246.
[15] G. C. Sedenho, D. De Porcellinis, Y. Jing, E. Kerr, L. Martin Mejia-Mendoza, Á. Vazquez-Mayagoitia, A. Aspuru-Guzik, R. G. Gordon, F. N. Crespilho, M. J. Aziz, *ACS Appl. Energ. Mater.* **2020**, *3*, 1933–1943.
[16] J. Montero, P. Navalpotro, A. D'Epifanio, B. Mecheri, S. Licoccia, J. Carretero-González, *J. Electroanal. Chem.* **2021**, *895*, DOI 10.1016/j.jelechem.2021.115442.
[17] P. Fischer, P. Mazúr, J. Krakowiak, *Molecules* **2022**, *27*, 560.
[18] Q. Chen, Y. Lv, Z. Yuan, X. Li, G. Yu, Z. Yang, T. Xu, Q. Chen, Y. Lv, Z. Yang, T. Xu, Z. Yuan, X. Li, G. Yu, *Adv. Funct. Mater.* **2021**, *32*, 2108777.
[19] M. Nourani, B. I. Zackin, D. C. Sabarirajan, R. Taspinar, K. Artyushkova, F. Liu, I. v. Zenyuk, E. Agar, *J. Electrochem. Soc.* **2019**, *166*, A353–A363.
[20] J. Chai, X. Wang, A. Lashgari, C. K. Williams, J. Jiang, *ChemSusChem* **2020**, *13*, 4069–4077.
[21] M. Bahari, G. D. Watt, J. N. Harb, *J. Electrochem. Soc.* **2021**, *168*, 090525.
[22] B. Hu, H. Fan, H. Li, M. Ravivarma, J. Song, B. Hu, H. Fan, H. Li, M. Ravivarma, J. Song, *Adv. Funct. Mater.* **2021**, *31*, 210273.
[23] T. Hagemann, J. Winsberg, M. Grube, I. Nischang, T. Janoschka, N. Martin, M. D. Hager, U. S. Schubert, *J. Power Sources* **2018**, *378*, 546–554.
[24] J. Luo, B. Hu, C. Debruler, T. L. Liu, *Angew. Chem. Int. Ed.* **2018**, *57*, 231–235; *Angew. Chem.* **2018**, *130*, 237–241.
[25] T. Liu, X. Wei, Z. Nie, V. Sprenkle, W. Wang, *Adv. Energy Mater.* **2016**, *6*, DOI 1501449.

[26] E. S. Beh, D. De Porcellinis, R. L. Gracia, K. T. Xia, R. G. Gordon, M. J. Aziz, J. A. Paulson, *ACS Energy Lett.* **2017**, *2*, 639–644.
[27] C. DeBruler, B. Hu, J. Moss, J. Luo, T. Leo Liu, *ACS Energy Lett.* **2018**, *3*, 663–668.
[28] B. Ambrose, R. P. Naresh, M. Ulaganathan, P. Ragupathy, M. Kathiresan, *Mater. Lett.* **2022**, *314*, 131876.
[29] P. S. Borchers, J. Elbert, I. Anufriev, M. Strumpf, I. Nischang, M. D. Hager, U. S. Schubert, P. S. Borchers, J. Elbert, I. Anufriev, M. Strumpf, I. Nischang, M. D. Hager, U. S. Schubert, *Macromol. Chem. Phys.* **2021**, *223*, 2100373.
[30] Y. Liu, Y. Li, P. Zuo, Q. Chen, G. Tang, P. Sun, Z. Yang, T. Xu, *ChemSusChem* **2020**, *13*, 2245–2249.
[31] A. Korshunov, A. Gibalova, M. Gruenebaum, B. Jan Ravoo, M. Winter, I. Cekic-Laskovic, *ACS Appl. Energ. Mater.* **2021**, *4*, 12353–12364.
[32] A. Korshunov, A. Gibalova, M. Grünebaum, B. J. Ravoo, M. Winter, I. Cekic-Laskovic, *Batteries & Supercaps* **2021**, *4*, 923–928.
[33] H. Li, H. Fan, B. Hu, L. Hu, G. Chang, J. Song, *Angew. Chem. Int. Ed.* **2021**, *60*, 26971–26977.
[34] L. Liu, Y. Yao, Z. Wang, Y. C. Lu, *Nano Energy* **2021**, *84*, 105897.
[35] A. Ohira, T. Funaki, E. Ishida, J.-D. Kim, Y. Sato, *ACS Appl. Energ. Mater.* **2020**, *3*, 4377–4383.
[36] X.-L. Lv, P. Sullivan, H.-C. Fu, X. Hu, H. Liu, S. Jin, W. Li, D. Feng, *ACS Energy Lett.* **2022**, *7*, 2428–2434.
[37] D. G. Kwabi, K. Lin, Y. Ji, E. F. Kerr, M. A. Goulet, D. De Porcellinis, D. P. Tabor, D. A. Pollack, A. Aspuru-Guzik, R. G. Gordon, M. J. Aziz, *Joule* **2018**, *2*, 1907–1908.
[38] J. Luo, A. Sam, B. Hu, C. DeBruler, X. Wei, W. Wang, T. L. Liu, *Nano Energy* **2017**, *42*, 215–221.
[39] B. Hwang, M.-S. Park, K. Kim, *ChemSusChem* **2015**, *8*, 310–314.
[40] C. G. Armstrong, R. W. Hogue, K. E. Toghill, *J. Electroanal. Chem.* **2020**, *872*, 114241.
[41] S. Hwang, H. seung Kim, J. H. Ryu, S. M. Oh, *J. Power Sources* **2018**, *395*, 60–65.
[42] D. Xu, C. Zhang, Y. Zhen, Y. Li, *ACS Appl. Energ. Mater.* **2021**, *4*, 8045–8051.
[43] Y. Li, Z. Xu, Y. Liu, S. Jin, E. M. Fell, B. Wang, R. G. Gordon, M. J. Aziz, Z. Yang, T. Xu, *ChemSusChem* **2021**, *14*, 745–752.
[44] S. Kim, D. Kim, G. Hwang, J. Jeon, *J. Electroanal. Chem.* **2020**, *869*, 114131.
[45] Y. Yao, H. Xu, Z. Tian, J. Zhang, F. Zhan, M. Yan, C. Jia, *ACS Appl. Energ. Mater.* **2021**, *4*, 8052–8058.
[46] B. R. Schrage, B. Zhang, S. C. Petrochko, Z. Zhao, A. Frkonja-Kuczin, A. Boika, C. J. Ziegler, *Inorg. Chem.* **2021**, *60*, 10764–10771.
[47] Q. Chen, Y. Li, Y. Liu, P. Sun, Z. Yang, T. Xu, *ChemSusChem* **2021**, *14*, 1295–1301.
[48] P. S. Borchers, M. Strumpf, C. Friebe, I. Nischang, M. D. Hager, J. Elbert, U. S. Schubert, *Adv. Energy Mater.* **2020**, *20*, 2001825.
[49] J. Yu, M. Salla, H. Zhang, Y. Ji, F. Zhang, M. Zhou, Q. Wang, *Energy Storage Mater.* **2020**, *29*, 216–222.
[50] Z. Zhao, B. Zhang, B. R. Schrage, C. J. Ziegler, A. Boika, *ACS Appl. Energ. Mater.* **2020**, *3*, 10270–10277.
[51] F. Valentini, F. Sabuzi, V. Conte, V. N. Nemykin, P. Galloni, *J. Org. Chem.* **2021**, *86*, 5680–5689.
[52] A. Vecchi, J. R. Sabin, F. Sabuzi, V. Conte, D. O. Cicero, B. Floris, P. Galloni, V. N. Nemykin, *Inorg. Chem.* **2021**, *60*, 8227–8241.
[53] F. Sabuzi, A. Coletti, G. Pomarico, B. Floris, P. Galloni, V. Conte, *J. Organomet. Chem.* **2019**, *885*, 49–58.
[54] G. A. Volpato, E. Colusso, L. Paoloni, M. Forchetta, F. Sgarbossa, V. Cristino, M. Lunardon, S. Berardi, S. Caramori, S. Agnoli, F. Sabuzi, P. Umari, A. Martucci, P. Galloni, A. Sartorel, *Photochem. Photobiol. Sci.* **2021**, *20*, 1243–1255.
[55] R. M. Nielson, J. T. Hupp, *Electron Self-Exchange Kinetics for a Water-Soluble Ferrocenium/Ferrocene Couple: Rate Modulation via Charge Dependent Calix[6]Arene-p-Sulfonate Encapsulation* **1996**.
[56] N. S. Lawrence, G. J. Tustin, M. Faulkner, T. G. J. Jones, *Electrochim. Acta* **2006**, *52*, 499–503.
[57] C. L. Bird, A. T. Kuhn, *Chem. Soc. Rev.* **1981**, *10*, 49–82.
[58] C. Debruler, B. Hu, J. Moss, J. Luo, T. L. Liu, *ACS Energy Lett.* **2018**, *3*, 663–668.
[59] M. Cuartero, R. G. Acres, J. Bradley, Z. Jarolimova, L. Wang, E. Bakker, G. A. Crespo, R. De Marco, *Electrochim. Acta* **2017**, *238*, 357–367.
[60] T. Liu, X. Wei, Z. Nie, V. Sprenkle, W. Wang, *Adv. Energy Mater.* **2016**, *6*, 1501449.
[61] E. S. Beh, D. de Porcellinis, R. L. Gracia, K. T. Xia, R. G. Gordon, M. J. Aziz, *ACS Energy Lett.* **2017**, *2*, 639–644.
[62] A. M. Tarr, D. M. Wiles, *Electronic Absorption Spectra and Photodecomposition of Some Substituted Ferrocenes'* **1968**.
[63] S. Hu, L. Wang, X. Yuan, Z. Xiang, M. Huang, P. Luo, Y. Liu, Z. Fu, Z. Liang, *Energy Mater. Adv.* **2021**, *2021*, 1–8.
[64] B. Hu, C. Debruler, Z. Rhodes, T. L. Liu, *J. Am. Chem. Soc.* **2017**, *139*, 1207–1214.
[65] L. R. F. Allen, J. Bard, *Electrochemical Methods* **2001**.
[66] R. S. Nicholson, *Anal. Chem.* **1965**, *37*, 1351–1355.
[67] C. Debruler, B. Hu, J. Moss, J. Luo, T. L. Liu, *ACS Energy Lett.* **2018**, *3*, 663–668.
[68] J. Yu, M. Salla, H. Zhang, Y. Ji, F. Zhang, M. Zhou, Q. Wang, *Energy Storage Mater.* **2020**, *29*, 216–222.
[69] G. Zotti, G. Schiavon, S. Zecchin, D. Favretto, *Dioxygen-Decomposition of Ferrocenium Molecules in Acetonitrile: The Nature of the Electrode-Fouling Films during Ferrocene Electrochemistry* **1998**.

Manuscript received: September 29, 2022
Revised manuscript received: November 7, 2022